Journal of Materials Chemistry B

Administration Sequence- and Formulation-dependent Vaccination using Acid-degradable Polymeric Nanoparticles with High Antigen Encapsulation Capability

Journal:	*Journal of Materials Chemistry B*
Manuscript ID	TB-ART-11-2023-002834.R2
Article Type:	Paper
Date Submitted by the Author:	14-May-2024

Complete List of Authors:	Choi, Yeon Su; University of California, Irvine Felgner, Jiin; University of California, Irvine Jan, Sharon; University of California, Irvine Davies, Jenny; University of California, Irvine Davies, D.; University of California Irvine, Physiology and Biophysics Kwon, Young Jik; University of California, Irvine, Pharmaceutical Sciences, and Chemical Engineering & Materials Science

ARTICLE

Administration Sequence- and Formation-dependent Vaccination using Acid-degradable Polymeric Nanoparticles with High Antigen Encapsulation Capability

Received 00th January 20xx,
Accepted 00th January 20xx

DOI: 10.1039/x0xx00000x

Yeon Su Choi,†[a] Jiin Felgner,†[a] Sharon Jan,[b] Jenny E. Hernandez-Davies,[b] D. Huw Davies*[b] and Young Jik Kwon*[acde]

Abstract. Vaccines aim to efficiently and specifically activate the immune system via a cascade of antigen uptake, processing, and presentation by antigen presenting cells (APCs) to CD4 and CD8 T cells, which in turn drive humoral and cellular immune responses. The specific formulation of the vaccine carriers can serve to not only shield the antigens from premature sequestering before reaching APCs but also favorably promote intracellular antigen presenting processing and presentation. This study compares two different acid-degradable polymeric nanoparticles that are capable of encapsulating moderately immunogenic antigen, GFP, at nearly full efficacy via electrostatic interactions or molecular affinity between His tag and Ni-NTA-conjugated monomers, resulting in GFP-encapsulating NPs composed of ketal monomers and crosslinkers (KMX/GFP NPs) and NTA-conjugated ketal monomers and crosslinkers (NKMX/GFP NPs), respectively. Encapsulated GFP was found to be released more rapidly from NKMX/GFP NPs (electrostatic encapsulation) than KMX/GFP NPs (affinity-driven encapsulation). *In vivo* vaccination studies demonstrated that while repeated injections of either NPs formulation resulted in poorer generation of anti-GFP antibodies than injections of the GFP antigen itself, sequential injections of NPs and GFP as a prime and booster vaccine, respectively, restored the humoral response. The results indicated that NPs primarily assist APCs to antigen presentation T cells, and B cells need to be further stimulated by free protein antigens to produce antibodies. The findings of this study suggest that the immune response can be modulated by varying the chemistry of vaccine carriers and the sequences of vaccination with free antigens and antigen-encapsulating NPs.

Key word: Polymeric vaccine carriers, antigen processing and presentation, humoral response, vaccination sequences, immune modulation

Introduction

Since its discovery, vaccination has played a pivotal role in improving human health. The demand for vaccines that can efficiently activate the immune system for a desired response against a pathogenic target has become greater than ever with the potential emergence of serious health threats, such as the recent COVID-19 pandemic.[1-5] Immune activation starts with introducing an antigen to antigen presenting cells (APCs) that can trigger the cascade of adaptive immunity, including humoral and cellular responses against the antigen.[6-10] Though many forms of antigenic proteins are poorly immunogenic upon administration, the design of efficient, safe, and versatile delivery carriers can overcome this limitation.[11-15] CD4 and CD8 T cells are prime targets of vaccination for their central roles in initiating the cascade of immune response.[16-18] Ideal vaccine carriers adeptly encapsulate antigens, effectively deliver and release them within in APCs, and facilitate the presentation of the antigenic peptides to targeted CD4 or CD8 T cells.

The molecular tunability of polymeric nanoparticles (NPs) for physical (e.g., size) and chemical (e.g., degradability) properties make them promising antigen and adjuvant carriers for versatile and efficient vaccination.[19-23] Their multifaceted function of efficient and facile encapsulation of antigens and intracellular release within APCs has been successfully employed for successful vaccination.[24-27] After uptake into APCs, exogenous protein antigens are degraded into peptides in endosomal compartments, which are in turn transported back

[a] *Department of Pharmaceutical Sciences, University of California, Irvine, CA 92697, United States. E-mail: kwonyj@uci.edu*
[b] *Vaccine Research and Development Center, University of California, Irvine, CA 92697, United States. E-mail: ddavies@uci.edu*
[c] *Department of Chemical and Biomolecular Engineering, University of California, Irvine, CA 92697, United States.*
[d] *Department of Biomedical Engineering, University of California, Irvine, CA 92697, United States.*
[e] *Department of Molecular Biology and Biochemistry, University of California, Irvine, CA 92697, United States.*
† Both authors contributed equally to this work.
Electronic Supplementary Information (ESI) available: [details of any supplementary information available should be included here]. See DOI: 10.1039/x0xx00000x

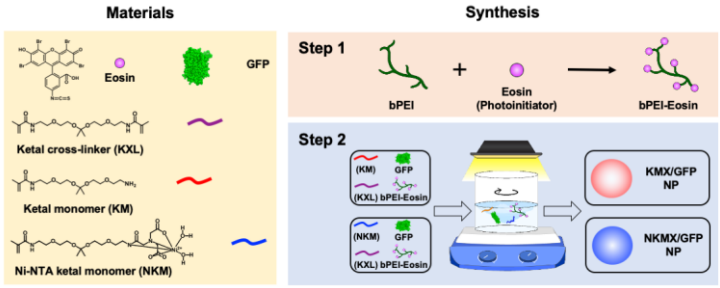

Figure 1. Synthesis scheme of KMX/GFP and NKMX/GFP NPs.

to the cell surface by class II MHC molecules for recognition by antigen receptors of CD4 T cells. In contrast, the transport of peptides by class I MHC molecules for recognition by CD8 T cells requires entry or origination of the antigen in the cytoplasm. Thus, a potentially useful property of polymeric NPs is assisting the antigen to escape from the endosomal pathway to the cytoplasm to promote both CD4 and CD8 activation. However, accomplishing loading of both class I and II MHC pathways remains a major technical challenge for polymeric NP vaccines.[28,29]

Conventional vaccines are repeatedly administered in the same formulations. Considering the diverse and distinct antigen processing and presentation pathways in generating humoral versus cellular immunity, vaccination with varying formulations in different orders could provide versatility and targeted immune activation. This proof-of concept study demonstrates the efficacy of acid-degradable polymeric NPs capable of efficiently encapsulating a broad range of recombinant protein antigens in their capacity of delivering the antigen payloads to APCs for antigen presentation to T cells toward immune modulations for targeted vaccination outcomes.

Results and discussion

Efficient encapsulation of GFP in relatively monodispersed KMX/GFP and NKMX/GFP NPs. Efficient vaccination requires a formulation with efficient versatile antigen encapsulation. His-tagged GFP was encapsulated in KMX/GFP and NKMX/GFP NPs, synthesized of acid-cleavable amino ketal methacrylamide monomer (KM), Ni-NTA ketal methacrylamide monomer (NKM), and ketal bismethacrylamide cross-linker (KXL), via attractive electrostatic interactions alone or in combination molecular affinity between His-tag and Ni-NTA, respectively (Figure 1 and Figure S1). GFP is known to be anionic at a neutral pH with a pKa of 6.0[30] and can be efficiently retained in a cationic molecular environment such as inside KMX NPs. Not all protein antigens are necessarily anionic, but many recombinant proteins are often His-tagged for separation and purification. Therefore, affinity-based protein encapsulation by Ni-NTA provides an opportunity to deliver a broad range of recombinant protein antigens. KM and NKM were pre-incubated with His-tagged GFP along with KXL, prior to photo-polymerization from the surface of eosin Y-conjugated PEI as illustrated in Figure 1. This surface-initiated photopolymerization enables synthetic flexibility of controlled, relatively monodispersed size, differential protein loading and differential structure construction, and free of GFP-free smaller particles, as previously validated.[31] Finally, the monomers and cross-linkers contain an acid-cleavable ketal linkage used for intracellular delivery of drugs, nucleic acids, and proteins in various applications.

The sizes of KMX/GFP and NKMX/GFP NPs were approximately 170 and 230 nm in diameter with relatively narrow size distributions indicated by polydispersity indices of 0.26 and 0.22, respectively (Figure 2a). The size of NKMX/GFP NPs was slightly larger than that of KMX/GFP, attributed to the relatively bulky Ni-NTA end of the NKM in comparison to KM with amino end of the KM (Figure 1). This observation also implies that charge of the KM was sufficient for electrostatic

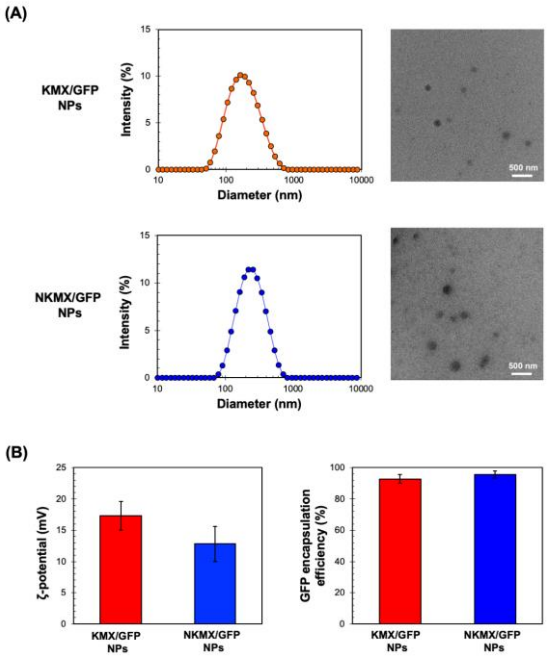

Figure 2. Characterized KMX/GFP and NKMX/GFP NPs by (a) size and morphology determined by DLS particle analysis and observed by TEM and (b) zeta-potential and GFP encapsulation efficiency (n=5).

interaction with a counter-charged protein. TEM images showed that both NPs were spherical in size with no aggregation (Figure 2a). As speculated, the incorporation of NKM to NPs decreased the surface charge (Figure 2b) from 17.3 mV (KMX/GFP NPs) to 12.8 mV (NKMX/GFP NPs) (Figure 2b). Regardless of the different molecular ratios of KM to NKM in both NPs, the majority of the His-tagged GFP was encapsulated with the efficiencies of approximately 93% and 96% in KMX/GFP and NKMX/GFP NPs, respectively. These results indicated that the incorporation of NKM in the NPs moderately improved the GFP encapsulation with an increased size and lowered surface charge.

GFP release from KMX/GFP and NKMX/GFP NPs at an endosomal pH. Antigens delivered to an antigen presenting cell (APC) are processed via endogenous or exogenous pathway, depending on their intracellular localizations.[32] Therefore, how rapidly antigens are released from NPs determines not only the overall antigen presentation efficacy but whether it is presented by MHC I or MHC II on the surface. At a physiological pH of 7.0, only a small fraction (10-15%) of encapsulated GFP was released from the NPs after 48 h, while a mildly acidic endosomal pH triggered much greater release of GFP (Figure 3a). In contrast to the similar releases at pH 7.0, a substantially higher amount of GFP was released from NKMX/GFP NPs (~ 69%) than KMX/GFP NPs (~ 36%) for 48 h. Notably, while the time required to reach a plateau of accumulated GFP release was almost identical for both NPs, there was an initial lag in GFP release from KMX/GFP NPs (Figure 3a). The almost 2-fold difference in overall GFP release between NPs and the greater initial GFP release from NKMX/GFP NPs can be attributed to a stronger attractive electrostatic interaction between the protonated amino end of KM at an acidic pH and GFP. Likewise, it was confirmed that approximately twice more GFP was still retained in the KMX/GFP NPs than in NKMX/GFP NPs when unreleased GFP was measured (data not shown). His-tagged

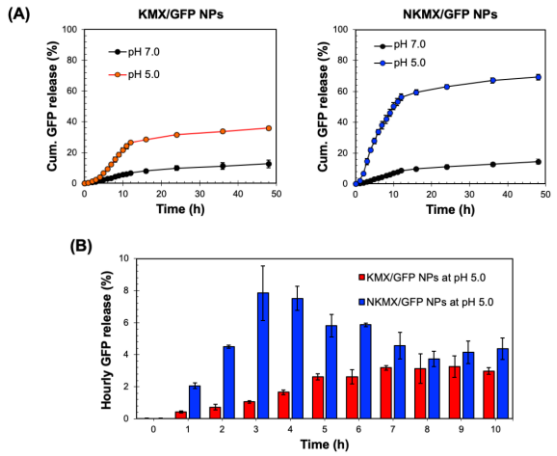

Figure 3. Acid-triggered release of GFP from KMX/GFP and NKMX/GFP NPs in DI water at 37 °C in a shaking incubator as (a) accumulated release for 48 h and (b) hourly release for the initial 10 h (mean ± SD; n=3).

GFP in NKMX/GFP NPs was released immediately upon the hydrolysis of ketal linkage, while the strengthened cationic environment KMX/GFP NPs retained GFP from rapid release. This outcome was further supported by the GFP detected per hour over the first 10 h (Figure 3b). This result demonstrated that GFP was released from NKMX/GFP NPs in rather a burst-like manner while KMX/GFP NPs released GFP in a sustained manner. The results in Figure 3 suggest a rapid release of GFP from NKMX/GFP NPs in the mildly acidic endosomes, possibly leading to fast degradation, in comparison to KMX/GFP NPs.

Intracellular trafficking of GFP release from KMX/GFP and NKMX/GFP NPs. Upon administration, vaccines are taken up by APCs, including macrophages and dendritic cells (DCs). While macrophages and DCs are known to be effective in degrading and salvaging antigens, the delivery of antigenic protein to them, especially in route to MHC I pathway, is challenging.[33,34] The intracellular distributions of GFP released from NPs in the nucleus, lysosome, or/and other places (e.g., cytoplasm) were tracked using a super resolution fluorescence microscope which is capable of imaging the morphology as narrow as ~ 20 nm.[35] The capability of acquiring the highest resolution images is traded off with inability of confocal imaging, which resulted in overlaid but pinpointed fluorescence location of GFP in the nuclei even at the highest intensity settings. The analysis showed that GFP quickly accumulated in the lysosome and cytoplasm while very little of it was found in the nucleus (Figures 4 and 5). Relative accumulation of GFP in the lysosome decreased with time, while its release into the cytoplasm increased, when delivered by KMX/GFP NPs. In contrast, GFP found in the lysosome increased with incubation time and its release into the cytoplasm decreased when NKMX/GFP NPs were incubated with RAW 264.7 cells, DC2.4 cells, and BMDCs (Figures 4 and 5). One possible explanation for this observation is stronger proton buffering and GFP retention by KMX NPs in the lysosome, resulting in faster cytosolic release of intact proteins (GFP). When delivered by NKMX/GFP NPs, GFP is quickly liberated into the reducing environment in the lysosome with slower release into the cytoplasm due to limited proton buffering. Previous studies also demonstrated that successful delivery of a therapeutic payload (e.g., proteins and nucleic acids) requires cytosolic release with avoided premature degradation and inactivation.[36,37] Relatively slower cellular uptake of NKMX/GFP NPs than KMX/GFP NPs, as indicated by mean fluorescence intensity (MFI), likely contributed to the slower cytosolic release (Figure 4 and 5). Antigen delivery in carriers such as NPs could be beneficial for extended bioavailability, avoided immediate immune response, and targeted uptake by phagocytic cells, which altogether can improve both vaccination efficacy and safety.[38,39] However, they would require utilizing an energy-dependent route (e.g., macropinocytosis) or via a structurally challenging uptake process (e.g., different membrane potential).[40-42] In contrast to NPs that contained multiple GFP proteins inside, free GFP

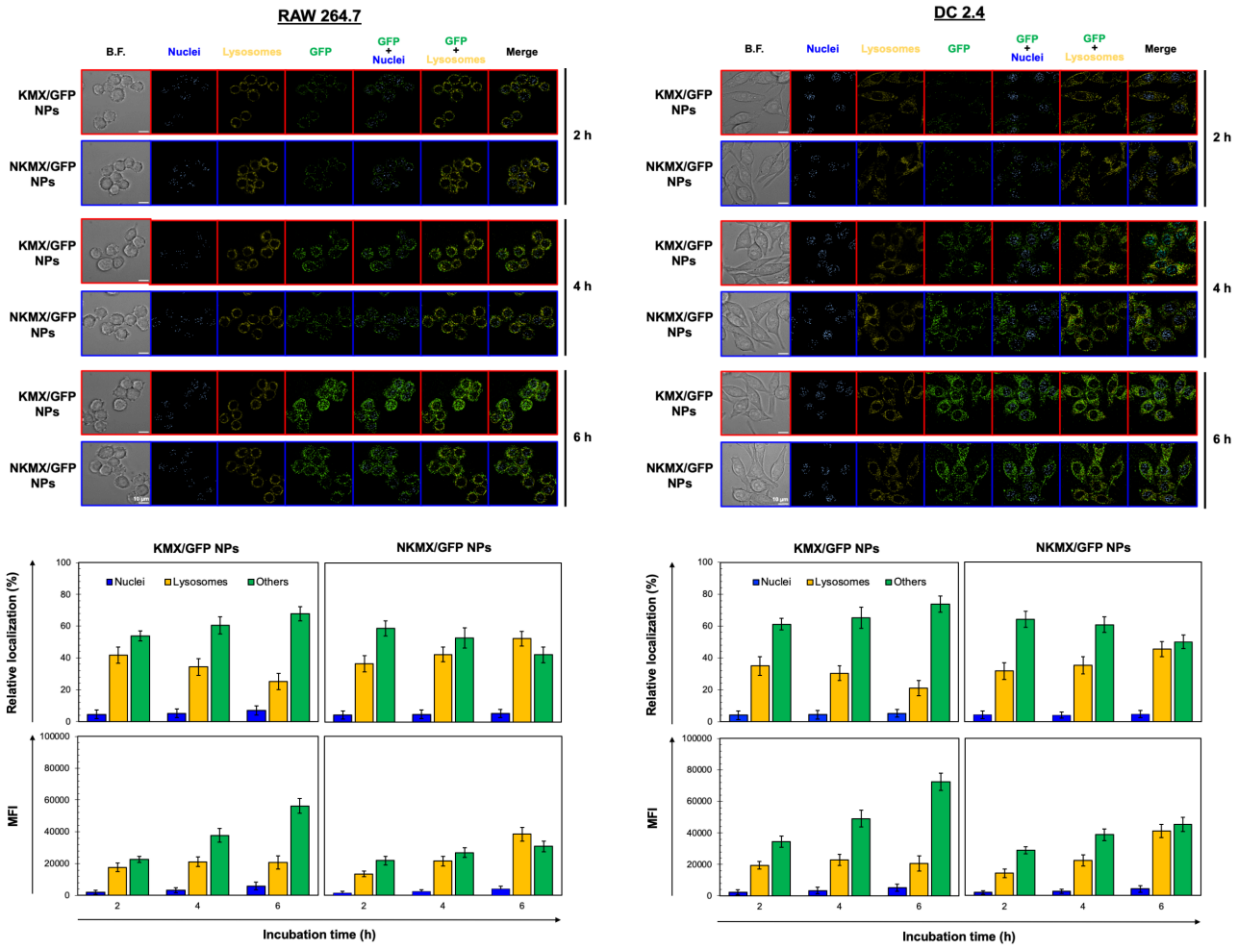

Figure 4. Intracellular distributions and accumulation of GFP delivered by KMX/GFP and NKMX/GFP NPs in RAW 264.7 and DC 2.4 cells for 2, 4, and 6 h. The fluorescence of GFP in the cells was imaged by super resolution fluorescence microscopy (image n=8–10) and co-localized fluorescence of GFP and intracellular organelles were further quantified. In addition, the cellular uptake of KMX/GFP and NKMX/GFP NPs was quantified as indicated by mean fluorescence intensity (MFI).

proteins parsley distributed in a cell were not highly visible (Figure S2). When incubated with RAW 264.7 cells, DC 2.4 cells, and BMDCs, KMX/GFP and NKXM/GFP NPs were found to be minimally toxic with relative viability of RAW 264.7 cells at ~ 91 and ~ 71%, DC 2.4 cells at ~ 89 and ~ 62%, and BMDCs at ~94 and 86%, respectively, at the highest concentration of 200 μg/mL of NPs (Figure S3). Despite the lower zeta-potential than KMX/GFP NPs (Figure 2b), Ni-NTA groups in NKMX/GFP NPs contributed to the cytotoxicity.[43] At a concentration of 100 μg/mL, KMX/GFP and NKMX/GFP NPs showed tolerable cytotoxicity of 20% or lower, allowing vaccination at a dose of up to 0.3 μg/mL of antigens. Incubation of BMDCs with KMX/GFP and NKMX/GFP NPs induced maturation, as indicated by upregulated expression of MHC II, CCR7, CD80, and CD86 (Figure 5). This attributed to the elevated antigen processing antigen presentation activities when NP vaccines are taken up by BMDCs.[44] In contrast, RAW 264.7 macrophages showed only a marginally upregulated CCR7, and DC 2.4 cells remained unchanged for expression of surface markers (Figures S4 and S5). This observation implies efficient DC activation in vivo upon vaccination by KMX/GFP and NKMX/GFP NPs.

Immune response determined by the order of vaccination in varying formulations. In vivo studies allow the assessment of humoral immunity initiated by antigen presentation to T cells. C57BL/6 mice, a common animal model in immunology, were vaccinated with 5 μg GFP, KMX/GFP NPs, or NKMX/GFP NPs in PBS, in various combinations of GFP and NPs for prime (Day 0) and booster (Day 14) injections, with or without IVAX-1 adjuvant (CpG/MPLA/AddaVAX) (Figure 6 and Figure S6). The animals were bled on Day 10 (after the prime but before the booster injection), Day 28 (2 weeks after the booster injection), and Day 50 (~ a month after complete vaccination), followed by evaluating the generation of antibodies against GFP by ELISA. Robust anti-GFP IgG responses were induced by vaccination with GFP-GFP, KMX/GFP NPs-GFP, and NKMX/GFP NPs-GFP (prime-booster) and the efficiently activated humoral immunity lasted about a month with no changes. No difference in

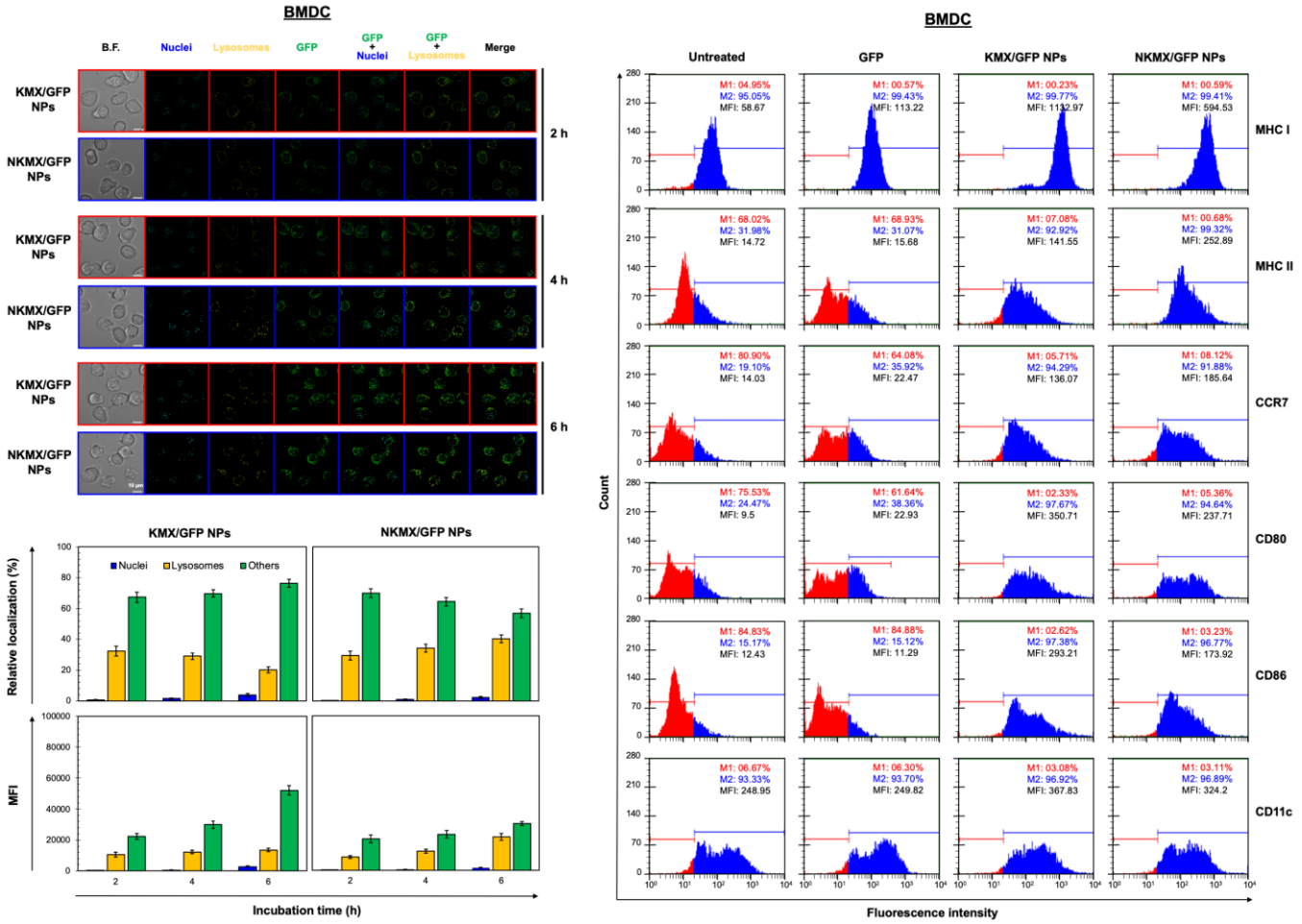

Figure 5. Intracellular distributions and accumulation of GFP delivered by KMX/GFP and NKMX/GFP NPs in BMDCs for 2, 4, and 6 h and the changes of cell surface markers on BMDCs after the incubation with KMX/GFP and NKMX/GFP NPs . The fluorescence of GFP in the cells was imaged by super resolution fluorescence microscopy (image n=7–9) and co-localized fluorescence of GFP and intracellular organelles were further quantified. In addition, the cellular uptake of KMX/GFP and NKMX/GFP NPs was quantified as indicated by mean fluorescence intensity (MFI). The cell surface markers on BMDCs after the incubation with free GFP, KMX/GFP NPs, and NKMX/GFP NPs for 6h were analyzed by flow cytometry.

IgG2a/IgG1 ratios observed between KMX/GFP NPs and NKMX/GFP NPs (Figure S7) confirmed their same roles in the Th1- or Th2-biased polarization of humoral immunity**.** In contrast, administration of KMX/GFP NPs and NKMX/GFP NPs for both prime and boost injections did not yield measurable antibodies, consistent with the notion that the antigen is sequestered inside the NPs until endocytosed and intracellularly degraded in an APC. Processed peptides are the presented in the context of MHC molecules to T cells at the APC surface. This finding emphasized the importance of administering soluble antigen (GFP), in the prime and/or boost, for inducing antibodies. It was demonstrated that administration of NPs for prime followed by soluble GFP for boost induced higher IgG signals than groups in which soluble GFP was given first. This may indicate a role for the NPs in modulating the antibody response via the prime injection. Overall, the production of anti-GFP antibodies by NPs was not as effective as that by free GFP. This might be attributed to the higher number of free proteins than NPs for the same amount of GFP, which also attribute to the relatively low statistical differences among the treatment groups and warrants a subsequent study at a higher dose than that used in the current study. Regardless of the formulations, IVAX-1 was indispensable for efficient antibody generation against a relatively weak antigen such as GFP. Further studies are required to define more precisely the potential for these NPs to enhance or downregulate both T cell and antibody responses. In particular, conventional vaccination strategies repeatedly administer the same formulations in prime and boost(s). However, the results shown in Figures 6 indicate the possibility of modulating the immune response by varying the immunization sequence with varying formulations.

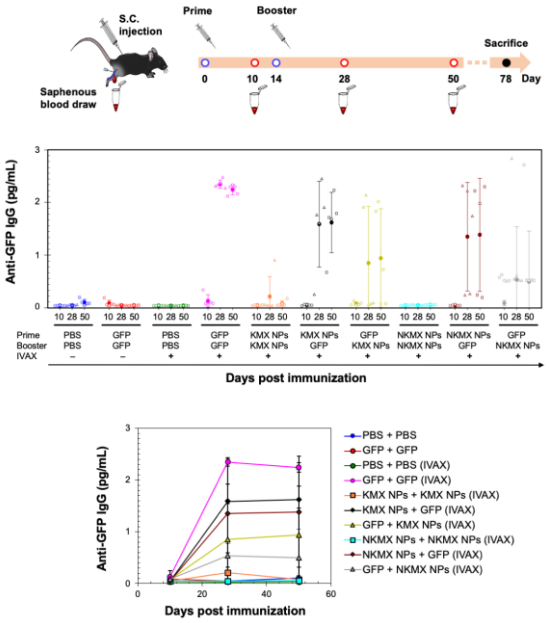

Figure 6. Humoral response to GFP, KMX/GFP NPs, and NKMX/GFP NPs in varying combinations of prime and booster injections. C57BL/6 mice were vaccinated twice on 14 days, and their blood samples were collected on Day 10, 28, and 50 and for the analysis of anti-GFP antibodies by ELISA (n=5).

Hypothesis of humoral immune response by antigen formulations in varying administration orders. Antigen presentation by an APC to T cells plays pivotal roles in orchestrating adaptive immunity, including humoral and cellular responses, which is the prime target in achieving efficient vaccination. The results of this study hinted that the magnitudes and types of immune response could be modulated by antigen formulations (soluble vs. encapsulated) and the sequence of their administration (summarized in Figure 7). Free proteins circulate upon injection before being internalized by an APC mainly via micropinocytosis[45], degraded in the lysosome into peptides, and loaded onto MHC II for antigen presentation[46] that are required for B cell-mediated antibody production. KMX/GFP and NKMX/GFP NPs used in this study protect their cargo upon administration, rapidly degrade in the mildly acidic lysosome of an APC after endocytosis, and rapidly release their payload not only to the lysosome but also the cytoplasm (Figures 4 and 5). Free antigens are also available to bind to the corresponding antigen receptors on B cells that differentiate into antibody-secreting plasma cells with cognate help from CD4 T cells. When GFP was delivered as free protein, its antigenic peptides were presented to CD4 T cells and simultaneously to B cells. When administered again as booster, it is processed for the same purpose and simultaneously bind to the B cells that are already primed from the prior vaccination, generating a strong humoral response including secreting antibodies (the first scenario in Figure 7). We propose that GFP delivered by acid-degradable NPs are processed in an APC and

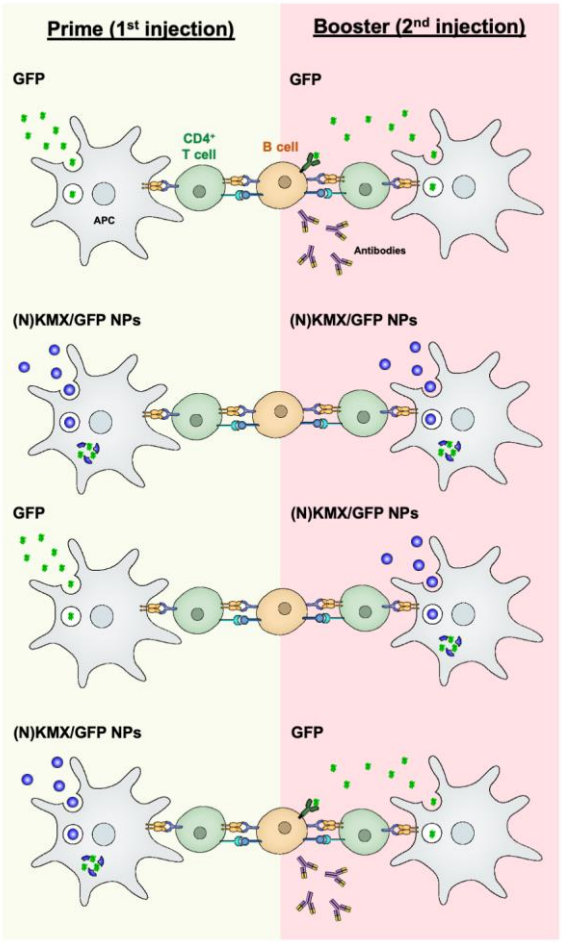

Figure 7. Schematic showing hypothesized modulation of the humoral immune response by alternating the administration of free antigens and antigen-encapsulating NPs.

processed GFP peptides are presented to CD4 cells, required for B cell differentiation. Repeated vaccination with GFP-encapsulating NPs does not provide free GFP to stimulate activated B cells (the second scenario in Figure 7). When GFP is delivered in NPs for booster, B cells that are activated upon prime injection of GFP do not get activated to become antibody-producing plasma cells (the third scenario in Figure 8). It is proposed that GFP released from NPs in an APC are processed and presented as peptides to CD4 T cells. Booster injection of free GFP enables the activation of B cells to differentiate to plasma cells (the fourth scenario in Figure 8). The results of this study direct us to develop vaccine strategies for the activation of humoral immunity. The findings presented in this study indicate that the administration of varying antigen formulations for prime and booster injections could improve strategies for achieving efficient and targeted vaccination. Studies are underway to test whether this platform, when used to deliver immunodominant antigens from specific pathogens, can influence immunogenicity, particularly for broadening antibody profiles, and improving efficacy against challenge. One of the

areas to be investigated in a subsequent study is to determine whether KMX/GFP and NKMX/GFP NPs affects the Th1- vs. Th2-biased polarization of humoral immunity, which may provide a new insight in molecularly modulating the immune systems to generate desired modes of immune response.

Conclusions

Successful vaccination is measured by the magnitude and types of immune response to the target antigen. In this study, a model antigen (GFP) was encapsulated in acid-degradable polymeric NPs via electrostatic interactions and molecular affinity. The resulting vaccine carriers were shown in vitro to release the antigen payload once internalized by an APC in response to the mildly acidic lysosome. Interestingly, the magnitude and quality of the immune response in mice were greatly affected by antigen formulation and vaccination sequence. While repeated vaccination with antigenic protein was most efficient in eliciting immune response, only limited humoral immunity was observed when antigen-encapsulating NPs were used for both prime and booster injections. Alternating free antigens and antigen-encapsulating NPs for prime and booster injections generated qualitatively different antibody productions, which is indicative of modulating the immune response by this approach. The findings of this study suggest the efficacy of a vaccine could be affected by the immunological nature of an antigen and its delivery carriers. For example, GFP used in this study is weakly immunogenic and the magnitude of immune response observed in this study is likely affected by the immunogenic nature of different antigens. The current proof-of-concept study needs to further be extended to investigating the roles of more common antigens such as ovalbumin, hemagglutinin, viral surface antigens (e.g., gp120 on HIV and SARS-CoV-2 spike proteins. Likewise, the polymeric NPs used in this study intracellularly release GFP in an APC. Vaccination with antigen-encapsulating NPs with different intracellular behaviors such as stimuli-responsive degradability and localization might show different traits of stimulating and modulating immune response. Overall, this study suggests that versatile strategies, including formulations and sequence, need to be considered in order to accomplish efficient and targeted vaccination.

Experimental

Materials. Branched polyethylenimine (bPEI, 25 kDa) and Hoechst 33342 dye were purchased from Sigma-Aldrich (St. Louis, MO). Eosin-5- isothiocyanate and LysoTracker™ Red DND-99 dye were purchased from Thermo Fisher Scientific (Waltham, MA). RAW 264.7 murine macrophage cells and DC 2.4 murine dendritic cells (ATCC, Rockville, MD) were cultured in Dulbecco's modification of Eagle's medium (DMEM) and RPMI 1640 (MediaTech, Manassas, VA), respectively, with 10% fetal bovine serum (FBS) (Atlanta Biologicals, Flowery Branch, GA) and 1% antibiotics (100 units/mL penicillin; 100 µg/mL streptomycin) (Gibco, Grand Island, NY) at 37 °C, 5% CO_2, and 95% humidity. AddaVAX™ (squalene oil-in-water emulsion) was purchased from InvivoGen (San Diego, CA). TLR9 agonist, CpG 1018-ODN, and TLR4 agonist, monophosphoryl lipid A (MPLA), were purchased from Integrated DNA Technologies (Coralville, Iowa) and Avanti Polar Lipids (Alabaster, AL), respectively. GFP with 6-His tag was expressed in Escherichia coli BL21 and purified by His-Pur Ni-NTA resin chromatography and Triton-X114 endotoxin removal. Purified proteins were evaluated by SDS-PAGE gel and bicinchoninic acid (BCA) protein assay (Pierce Biotechnology, Rockford, IL).

Preparation and characterization of KMX/GFP and NKMX/GFP nanoparticles (NPs). Acid-degradable NPs were synthesized via surface-initiated photo-polymerization of acid-degradable amino-ketal methacrylamide (KM) and Ni-NTA-ketal methacrylamide (NKM) monomers (Figure S1), and ketal bismethacrylamide crosslinker (KXL), for electrostatic or affinitive encapsulation of GFP as an antigen (Figure 1) as described in the Supplementary Information in detail. For the synthesis of KMX/GFP NPs, 20 µL of 100 mg/mL KM (2 mg), 10 µL of 100 mg/mL KXL (1 mg), 10 µL of 1 mg/mL GFP (10 µg), and 50 µL of 200 mg/mL ascorbic acid (10 mg), all in deionized (DI) water, were mixed with 910 µL of 86.4 µg/mL PEI-eosin conjugate dropwise, a total mixing volume of 1 mL, with vigorous stirring for 10 min. For the synthesis of NKMX/GFP NPs, 20 µL of 100 mg/mL Ni-NTA-KM (2 mg), 10 µL of 100 mg/mL KXL (1 mg), 10 µL of 1 mg/mL GFP (10 µg), and 50 µL of 200 mg/mL ascorbic acid (10 mg) were also mixed with 910 µL of 86.4 µg/mL PEI-eosin conjugate in the same way. Then, the mixture was photo-polymerized under a halogen lamp at 700 klux for 10 min with vigorous stirring, followed by additional stirring for 10 min without the light. Unreacted monomers, crosslinkers, and other reagents were removed by centrifugal filtration (MWCO 100 kDa, Millipore, Bedford, MA) three times at 3,000g and 4 °C for 10 min. The resulting KMX/GFP and NKMX/GFP NPs were finally re-suspended in 1 mL DI water and stored at 4 °C before being used for further studies.

The size and zeta-potential of KMX/GFP and NKMX/GFP NPs were measured using a dynamic light scattering (DLS) particle analyzer, Zetasizer Nano ZS (Malvern Panalytical, Malvern, UK), with a refractive index of 1.59 and an absorption of 0.01 at 25 °C. For 1 mL of KMX/GFP and NKMX/GFP NPs at a concentration of 10 µg His-tagged GFP/mL, each size measurement was conducted with a series of 15 runs using disposable cuvettes (ZEN0040, Malvern Panalytical) for size and each zeta-potential analysis was conducted with a series of 100 runs using DTS1070 folded capillary cells (Malvern Panalytical). The morphology of the KMX/GFP and NKMX/GFP NPs was observed by transmission electron microscopy (TEM). Briefly, 10 µL KMX/GFP or NKMX/GFP NPs at the concentration used for DLS and zeta-potential analysis were dropped on a carbon-coated copper grid (Thermo Fisher Scientific), air-dried for 30 min at

room temperature, and observed under a JEOL 2100F transmission electron microscope (JEOL, Peabody, MA) at 200 kV. The encapsulation efficiency of His-tagged GFP in KMX/GFP and NKMX/GFP NPs was determined by measuring the GFP's excitation/emission (390 nm/510 nm) of released GFP following hydrolysis using a fluorescence spectrometer (Synergy H1, BioTek, VT). The KMX/GFP and NKMX/GFP NPs were hydrolyzed in a 100 mM acetate buffer at pH 5.0 with vigorous stirring at room temperature for 24 h. The released GFP was determined by comparing the hydrolyzed samples with a calibration curve of free His-tagged GFP in DIW at a concentration range of 0 - 20 μg/mL.

pH-triggered GFP release from KMX/GFP and NKMX/GFP NPs. The release of His-tagged GFP from the KMX/GFP and NKMX/GFP NPs in a pH-dependent manner was evaluated by measuring the fluorescence of free GFP at the endosomal/phagolysosomal and physiological pH of 5.0 and 7.4, respectively. Briefly, a Spectra-Por® Float-A-Lyzer® G2 dialysis devices (MWCO 100 kDa) (Sigma-Aldrich) containing KMX/GFP and NKMX/GFP NPs at a concentration of 5 μg/mL GFP in 100 mM acetate buffer (pH 5.0) were incubated on a shaker incubator at 37 °C. At different time points, dialyzed samples in 4 mL were collected, while replenishing the buffers were replenished in the same volume, and analyzed for fluorescence using a Synergy H1 Microplate Fluorescence Reader (Synergy H1, BioTek, VT) at excitation/emission at 385 nm/524 nm (pH 5.0) or 390 nm/510 nm (pH 7.4) wavelengths, without further dilution or reconstitution. The released GFP amount was calculated by comparing the fluorescence of GFP at known concentrations as used above.

Cytotoxicity and intracellular distribution of KMX/GFP and NKMX/GFP NPs. The dose-dependent toxicity of KMX/GFP and NKMX/GFP NPs in vitro was assessed at concentrations of up to 200 μg/mL by the conventional MTT assay using RAW 264.7 cells, DC 2.4 cells, and BMDCs[47] seeded at a density of 10,000 cells per well in a 96-well plate with 0.1 mL medium, 24 h prior to the experiment. After the cells were incubated with KMX/GFP and NKMX/GFP NPs for 24 h, 10 μL of 5 mg/mL MTT in PBS was added to each well, followed by further incubation for 2 h. The MTT-containing medium was aspirated, 0.2 mL of DMSO was added to dissolve the formazan crystals produced by the live cells, and the absorbance of the formazan was measured at 570 nm using a SpectraMax Plus microplate reader (Molecular Devices, Sunnyvale, CA). The relative viability of the cells was determined by comparing the absorbance of the treated to untreated cells.

The intracellular distribution of His-tagged GFP delivered by KMX/GFP and NKMX/GFP NPs was evaluated using a Nanoreso™ Super Resolution Fluorescence Microscope (Sysmex Corporation, Kobe, Japan). Briefly, 20,000 of RAW 264.7 and DC 2.4 cells were seeded in a 8-well chamber dish (Thermo Fisher Scientific, Walham, MA) and incubated for 24 h. After incubation with KMX/GFP and NKMX/GFP NPs at a GFP concentration of 1 μg/mL for 2, 4, and 6 h, the cells were stained with LysoTracker™ Red DND-99 at a concentration of 100 nM for 20 min order to locate acidic intracellular organelles, while their nuclei were stained with Hoechst 33342 at a concentration of 1 μg/mL for 10 min. The cells were rinsed with DPBS twice and the fluorescence of GFP in the cells was captured in 10,000 frames per image. The location of intracellular GFP and other fluorophores was precisely determined by analyzing the obtained images using ThunderSTORM for image filtering with a wavelet filter (B-Spline) and result visualization by normalized Gaussian method and colocalized fluorescence, located in the same location, and then was quantified (% volume colocalized) using Image J software (National Institutes of Health, Bethesda, MD; https://imagej.nih.gov/ij/.) in analysis mode.

Analysis by cell surface molecules afrer incubation with KMX/GFP and NKMX/GFP NPs. The sell urface molecules after incubation with KMX/GFP and NKMX/GFP NPs were measured by flow cytometry. Briefly, RAW 264.7, DC2.4, and immature BMDCs were seeded at a density of 200,000 per well in a 12-well plate 24 h prior to the experiment. After 6 h incubation with GFP, KMXGFP, or NKMX/GFP NPs at a concentration of 1 μg/mL GFP or equivalent, the cells were trypsinized and stained with PE-Cy7 anti-mouse antibodies against MHCI, MHCII, CCR7, CD80, CD86 or CD11c (BioLegend, San Diego, CA) on ice for 20 min. The cells were then rinsed with 1X PBS three times and analyzed by flow cytometry using the unlabelled samples as controls.

Vaccine adjuvant preparation. In preparation of IVAX-1, a customized adjuvant mixture used in this study, CpG1018-ODN[48,49] was dissolved in sterile water at 1 mM as stock. To overcome the limited aqueous solubility, MPLA was incorporated into DOPG liposomes (an inert co-lipid). Briefly, MPLA and DOPG (both from Avanti Polar Lipids, Alabaster, AL) were dissolved at a molar ratio of 1:5 in chloroform, followed by evaporation under nitrogen and removal overnight under vacuum. The lipid film was then hydrated with 10 mM NaCl to a concentration of 5 mg/mL (2.835 mM) MPLA and sonicated in a Branson M1800 sonicating water bath (Branson Ultrasonics Corporation, Brookfield, CT) at room temperature for 15 min until the formulation was translucent with no large visible particles. Particle size distribution of the liposomes was found to be approximately 100 nm by DLS. AddaVAX™ (squalene oil-in-water emulsion, Invitrogen Inc., San Diego, CA) was used in 50% of the dosing volume in adjuvanted formulations as recommended by the manufacturer. In this study, mice received IVAX-1 comprised of 1 nmole CpG1018-ODN, 3 nmole MPLA, and 25 μL AddaVax as the adjuvant. IVAX-1 was developed and well characterized at UCI Vaccine R&D Center after performing systematic screens of different toll-like receptor (TLR) agonists and emulsions on the immunogenicity of recombinant hemagglutinin (HA) vaccines in mice.[49]

Vaccination by KMX/GFP and NKMX/GFP NPs. Female C57BL/6 mice (7-10 weeks of age) purchased from Charles River Laboratories (Wilmington, MA) received vaccines comprised of either free soluble His-tagged GFP or His-tagged GFP encapsulated in KMX/GFP or NKMX/GFP NPs as prepared above. For immunization, a dose of 5 μg of His-tagged GFP or equivalent in 50 μL was administered in sterile PBS or in IVAX-1 adjuvant via subcutaneous route (base of tail) under brief anesthesia with inhaled 1% isoflurane/O_2 mixture. Mice were weighed and monitored daily for 14 days post prime or boost for any changes in behavior or development of lesions as the site of injection. At regular time points, plasma was collected into heparinized microcapillary tubes (Minicollect 0.8 mL Z Serum Sep Gold, Greiner Bio-One, Monroe, NC) by saphenous vein bleed under anesthesia with inhaled 1% isoflurane/O_2 and at the experimental endpoint by cardiac puncture under terminal anesthesia. All animal work was approved by the UCI Institutional Animal Care and Use Committee (IACUC protocol #AUP-18-096) and by the Animal Care and Use Review Office (ACURO) of the U.S. Army Medical Research and Materiel Command (USAMRMC). The laboratory animal resources at UCI are internationally accredited by the Association for Assessment and Accreditation of Laboratory Animal Care (AAALAC #000238).

Anti-GFP antibody quantification by ELISA. His-tagged GFP was used to coat Reacti-Bind microtiter plates (Thermo Fisher Scientific, Waltham, MA) at a concentration of 2 μg/mL in TBS (20 mM Tris/150 mM NaCl, pH 7.6; 100 μL/well) overnight at 4 ^{o}C. The plates were then washed four times with T-TBS, TBS containing 0.05% Tween 20 (Thermo Fisher Scientific, Walham, MA) and blocked with 300 μL/well of casein/TBS blocking buffer (Thermo Fisher Scientific, Walham, MA) for 1-2 h. The blocking buffer was then aspirated and the plates were air-dried and stored in desiccated foil pouches at 4 ^{o}C until use. For the ELISA assay, sera were diluted to 1/100 in casein/TBS blocking buffer containing E. coli lysate (GenScript, Piscataway, NJ) at 1.5 mg/mL final concentration and incubated for 30 min prior to adding into the plates. Plates were incubated for 45 min with gentle rocking at room temperature. After washing with T-TBS four times, 100 μL of goat anti-human IgG, IgG1 or IgG2c-HRP conjugates (Bethyl Laboratories, Montgomery, TX) diluted to 1/12,500 in Guardian Stabilizer (Thermo Fisher Scientific, Walham, MA) was added to wells and incubated for 45 min at room temperature. After washing with T-TBS four more times, plates were developed by adding 100 μL/well SureBlue Reserve TMB developer (Kirkegaard and Perry Laboratories, Gaithersburg, MD) for 2-5 min in the dark. Development was stopped by the addition of 100 μL/well of 0.2 M H_2SO_4 and absorbance at 450 nm was measured using a FilterMax-F5 plate reader (Molecular Devices, San Jose, CA).

Statistical analysis. All data were analyzed for statistical significance using unpaired Student's *t*-test for single comparison at $p < 0.05$, $p < 0.01$, or $p < 0.001$.

Author Contributions

Yeon Su Choi: Conceptualization, Methodology, Validation, Formal analysis, Investigation, Writing – drafting, review, and editing, Visualization; **Jiin Felgner**: Validation, Formal analysis, Investigation, Writing – drafting, review, and editing; **Sharon Jan**: Methodology, Validation, Formal analysis; **Jenny E. Hernandez-Davies**: Methodology, Validation, Formal analysis, Investigation; **D. Huw Davies**: Validation, Formal analysis, Investigation, Writing – review and editing, Supervision; **Young Jik Kwon**: Conceptualization, Methodology, Writing - Original Draft, Writing – revised draft, Writing – review and editing, Supervision, Visualization, Project administration

Conflicts of interest

There are no conflicts to declare.

Acknowledgements

This work was supported by Defense Threat Reduction Agency (DTRA) grant HDTRA1-18-1-0036 and a research gift from Pharma Research, Co., Ltd. The authors thank Olivia Ritchie and Rebecca Lee for proofreading the manuscript.

Notes and references

§ Electronic supplementary information (ESI) available. See DOI: [link to be added].

1 F. P. Polack, S. J. Thomas, N. Kitchin, J. Absalon, A. Gurtman, S. Lockhart, J. L. Perez, G. Perez Marc, E. D. Moreira, C. Zerbini, R. Bailey, K. A. Swanson, S. Roychoudhury, K. Koury, P. Li, W. V. Kalina, D. Cooper, R. W. Frenck, Jr., L. L. Hammitt, O. Tureci, H. Nell, A. Schaefer, S. Unal, D. B. Tresnan, S. Mather, P. R. Dormitzer, U. Sahin, K. U. Jansen, W. C. Gruber and C. C. T. Group, *N Engl J Med*, 2020, **383**, 2603-2615.

2 J. Yang, W. Wang, Z. Chen, S. Lu, F. Yang, Z. Bi, L. Bao, F. Mo, X. Li, Y. Huang, W. Hong, Y. Yang, Y. Zhao, F. Ye, S. Lin, W. Deng, H. Chen, H. Lei, Z. Zhang, M. Luo, H. Gao, Y. Zheng, Y. Gong, X. Jiang, Y. Xu, Q. Lv, D. Li, M. Wang, F. Li, S. Wang, G. Wang, P. Yu, Y. Qu, L. Yang, H. Deng, A. Tong, J. Li, Z. Wang, J. Yang, G. Shen, Z. Zhao, Y. Li, J. Luo, H. Liu, W. Yu, M. Yang, J. Xu, J. Wang, H. Li, H. Wang, D. Kuang, P. Lin, Z. Hu, W. Guo, W. Cheng, Y. He, X. Song, C. Chen, Z. Xue, S. Yao, L. Chen, X. Ma, S. Chen, M. Gou, W. Huang, Y. Wang, C. Fan, Z. Tian, M. Shi, F. S. Wang, L. Dai, M. Wu, G. Li, G. Wang, Y. Peng, Z. Qian, C. Huang, J. Y. Lau, Z. Yang, Y. Wei, X. Cen, X. Peng, C. Qin, K. Zhang, G. Lu and X. Wei, *Nature*, 2020, **586**, 572-577.

3 N. Vabret, G. J. Britton, C. Gruber, S. Hegde, J. Kim, M. Kuksin, R. Levantovsky, L. Malle, A. Moreira, M. D. Park, L. Pia, E. Risson, M. Saffern, B. Salome, M. Esai Selvan, M. P. Spindler, J. Tan, V. van der Heide, J. K. Gregory, K. Alexandropoulos, N. Bhardwaj, B. D. Brown, B. Greenbaum, Z. H. Gumus, D. Homann, A. Horowitz, A. O. Kamphorst, M. A. Curotto de

Lafaille, S. Mehandru, M. Merad, R. M. Samstein and P. Sinai Immunology Review Project, *Immunity*, 2020, **52**, 910-941.
4 J. Y. Chung, M. N. Thone and Y. J. Kwon, *Adv Drug Deliv Rev*, 2021, **170**, 1-25.
5 A. Farlow, E. Torreele, G. Gray, K. Ruxrungtham, H. Rees, S. Prasad, C. Gomez, A. Sall, J. Magalhaes, P. Olliaro and P. Terblanche, *Vaccines (Basel)*, 2023, **11**, 690.
6 W. Tai, S. Feng, B. Chai, S. Lu, G. Zhao, D. Chen, W. Yu, L. Ren, H. Shi, J. Lu, Z. Cai, M. Pang, X. Tan, P. Wang, J. Lin, Q. Sun, X. Peng and G. Cheng, *Nat Commun*, 2023, **14**, 2962.
7 J. Liu, A. Chandrashekar, D. Sellers, J. Barrett, C. Jacob-Dolan, M. Lifton, K. McMahan, M. Sciacca, H. VanWyk, C. Wu, J. Yu, A. Y. Collier and D. H. Barouch, *Nature*, 2022, **603**, 493-496.
8 L. T. Gray, M. M. Raczy, P. S. Briquez, T. M. Marchell, A. T. Alpar, R. P. Wallace, L. R. Volpatti, M. S. Sasso, S. Cao, M. Nguyen, A. Mansurov, E. Budina, E. A. Watkins, A. Solanki, N. Mitrousis, J. W. Reda, S. S. Yu, A. C. Tremain, R. Wang, V. Nicolaescu, K. Furlong, S. Dvorkin, B. Manicassamy, G. Randall, D. S. Wilson, M. Kwissa, M. A. Swartz and J. A. Hubbell, *Biomaterials*, 2021, **278**, 121159.
9 D. J. Irvine, M. A. Swartz and G. L. Szeto, *Nat Mater*, 2013, **12**, 978-990.
10 S. N. Mueller, S. Tian and J. M. DeSimone, *Mol Pharm*, 2015, **12**, 1356-1365.
11 J. F. Correia-Pinto, N. Csaba and M. J. Alonso, *Int J Pharm*, 2013, **440**, 27-38.
12 J. W. Lim, W. Na, H. O. Kim, M. Yeom, A. Kang, G. Park, C. Park, J. Ki, S. Lee, B. Jung, H. H. Jeong, D. Park, D. Song and S. Haam, *J Mater Chem B*, 2020, **8**, 5620-5626.
13 P. Li, G. Shi, X. Zhang, H. Song, C. Zhang, W. Wang, C. Li, B. Song, C. Wang and D. Kong, *J Mater Chem B*, 2016, **4**, 5608-5620.
14 G. Liu, M. Zhu, X. Zhao and G. Nie, *Adv Drug Deliv Rev*, 2021, **176**, 113889.
15 M. F. Bachmann and G. T. Jennings, *Nat Rev Immunol*, 2010, **10**, 787-796.
16 J. Ning, Q. Wang, Y. Chen, T. He, F. Zhang, X. Chen, L. Shi, A. Zhai, B. Li and C. Wu, *J Med Virol*, 2023, **95**, e28743.
17 G. A. Koretzky, *J Immunol*, 2010, **185**, 2643-2644.
18 M. M. Painter, D. Mathew, R. R. Goel, S. A. Apostolidis, A. Pattekar, O. Kuthuru, A. E. Baxter, R. S. Herati, D. A. Oldridge, S. Gouma, P. Hicks, S. Dysinger, K. A. Lundgreen, L. Kuri-Cervantes, S. Adamski, A. Hicks, S. Korte, J. R. Giles, M. E. Weirick, C. M. McAllister, J. Dougherty, S. Long, K. D'Andrea, J. T. Hamilton, M. R. Betts, P. Bates, S. E. Hensley, A. Grifoni, D. Weiskopf, A. Sette, A. R. Greenplate and E. J. Wherry, *Immunity*, 2021, **54**, 2133-2142.e3.
19 C. Foged, B. Brodin, S. Frokjaer and A. Sundblad, *Int J Pharm*, 2005, **298**, 315-322.
20 R. R. Shah, M. Taccone, E. Monaci, L. A. Brito, A. Bonci, D. T. O'Hagan, M. M. Amiji and A. Seubert, *Sci Rep*, 2019, **9**, 11520.
21 G. P. Howard, G. Verma, X. Ke, W. M. Thayer, T. Hamerly, V. K. Baxter, J. E. Lee, R. R. Dinglasan and H. Q. Mao, *Nano Res*, 2019, **12**, 837-844.
22 E. R. Steenblock and T. M. Fahmy, *Mol Ther*, 2008, **16**, 765-772.
23 J. A. Cohen, T. T. Beaudette, W. W. Tseng, E. M. Bachelder, I. Mende, E. G. Engleman and J. M. J. Fréchet, *Bioconjugate Chemistry*, 2009, **20**, 111-119.
24 Q. Liu, X. Chen, J. Jia, W. Zhang, T. Yang, L. Wang and G. Ma, *ACS Nano*, 2015, **9**, 4925-4938.
25 C. Pan, L. Wang, M. Zhang, J. Li, J. Liu and J. Liu, *J Am Chem Soc*, 2023, **145**, 13261-13272.
26 Y. Li, A. W. Frei, E. Y. Yang, I. Labrada-Miravet, C. Sun, Y. Rong, M. M. Samojlik, A. L. Bayer and C. L. Stabler, *Biomaterials*, 2020, **256**, 120182.
27 P. O. Ilyinskii, C. J. Roy, C. P. O'Neil, E. A. Browning, L. A. Pittet, D. H. Altreuter, F. Alexis, E. Tonti, J. Shi, P. A. Basto, M. Iannacone, A. F. Radovic-Moreno, R. S. Langer, O. C. Farokhzad, U. H. von Andrian, L. P. Johnston and T. K. Kishimoto, *Vaccine*, 2014, **32**, 2882-2895.
28 S. Foster, C. L. Duvall, E. F. Crownover, A. S. Hoffman and P. S. Stayton, *Bioconjugate Chemistry*, 2010, **21**, 2205-2212.
29 R. Vyasamneni, V. Kohler, B. Karki, G. Mahimkar, E. Esaulova, J. McGee, D. Kallin, J. H. Sheen, D. Harjanto, M. Kirsch, A. Poran, J. Dong, L. Srinivasan, R. B. Gaynor, M. E. Bushway and J. R. Srouji, *Cell Rep Methods*, 2023, **3**, 100388.
30 B. C. Campbell, M. G. Paez-Segala, L. L. Looger, G. A. Petsko and C. F. Liu, *Nat Methods*, 2022, **19**, 1612-1621.
31 S. K. Cho, R. T. Lee, Y. H. Hwang and Y. J. Kwon, *ChemMedChem*, 2022, **17**, e202100718.
32 J. S. Blum, P. A. Wearsch and P. Cresswell, *Annu Rev Immunol*, 2013, **31**, 443-473.
33 E. M. Muntjewerff, L. D. Meesters and G. van den Bogaart, *Front Immunol*, 2020, **11**, 1276.
34 T. Zhang, A. Aipire, Y. Li, C. Guo and J. Li, *Biomedicine & Pharmacotherapy*, 2023, **168**, 115758.
35 D. Hara, S. N. Uno, T. Motoki, Y. Kazuta, Y. Norimine, M. Suganuma, S. Fujiyama, Y. Shimaoka, K. Yamashita, M. Okada, Y. Nishikawa, H. Amino and S. Iwanaga, *J Phys Chem B*, 2021, **125**, 8703-8711.
36 Y. J. Kwon, S. M. Standley, A. P. Goodwin, E. R. Gillies and J. M. J. Fréchet, *Molecular Pharmaceutics*, 2005, **2**, 83-91.
37 M. S. Shim, X. Wang, R. Ragan and Y. J. Kwon, *Microsc Res Tech*, 2010, **73**, 845-856.
38 P. Zamani, M. Mashreghi, M. Rezazade Bazaz, S. Zargari, F. Alizadeh, M. Dorrigiv, A. Abdoli, H. Aminianfar, M. Hatamipour, J. Zarqi, S. Behboodifar, Y. Samsami, S. Khorshid Sokhangouy, Y. Sefidbakht, V. Uskokovic, S. M. Rezayat, M. R. Jaafari and S. Mozaffari-Jovin, *J Control Release*, 2023, **360**, 316-334.
39 E. Yan Wang, M. Sarmadi, B. Ying, A. Jaklenec and R. Langer, *Biomaterials*, 2023, **303**, 122345.
40 C. C. Norbury, L. J. Hewlett, A. R. Prescott, N. Shastri and C. Watts, *Immunity*, 1995, **3**, 783-791.
41 Y. Shi, J. Huang, Y. Liu, J. Liu, X. Guo, J. Li, L. Gong, X. Zhou, G. Cheng, Y. Qiu, J. You and Y. Lou, *Science Advances*, 2022, **8**, eabo1827.
42 Z. Liu and P. A. Roche, *Front Physiol*, 2015, **6**, 1.
43 S. Latvala, J. Hedberg, S. Di Bucchianico, L. Moller, I. Odnevall Wallinder, K. Elihn and H. L. Karlsson, *PLoS One*, 2016, **11**, e0159684.
44 H. Zhao, Y. Li, B. Zhao, C. Zheng, M. Niu, Q. Song, X. Liu, Q. Feng, Z. Zhang and L. Wang, *Acta Pharm Sin B*, 2023, **13**, 3892-3905.
45 J. C. Charpentier and P. D. King, *Cell Commun Signal*, 2021, **19**, 92.
46 P.A. Roche and K. Furuta, *Nat Rev Immunol*, 2015, **15**, 203-217.
47 M. N. Thone, J. Y. Chung, D. Ingato, M. L. Lugin and Y. J. Kwon. *Adv Ther* 2023, **6**, 2200125
48 J. E. Hernandez-Davies, J. Felgner, S. Strohmeier, E. J. Pone, A. Jain, S. Jan, R. Nakajima, A. Jasinskas, E. Strahsburger, F. Krammer, P. L. Felgner and D. H. Davies, *Front Immunol*, 2021, **12**, 692151.
49 J. E. Hernandez-Davies, E. P. Dollinger, E. J. Pone, J. Felgner, L. Liang, S. Strohmeier, S. Jan, T. J. Albin, A. Jain, R. Nakajima, A. Jasinskas, F. Krammer, A. Esser-Kahn, P. L. Felgner, Q. Nie and D. H. Davies, *Sci Rep*, 2022, **12**, 9198.